Directional velocity estimation using a spatio-temporal encoding technique based on frequency division for synthetic transmit aperture ultrasound

Gran, Fredrik; Jensen, Jørgen Arendt

Published in:
I E E E Transactions on Ultrasonics, Ferroelectrics and Frequency Control

Link to article, DOI:
10.1109/TUFFC.2006.1665077

Publication date:
2006

Document Version
Publisher's PDF, also known as Version of record

Directional Velocity Estimation Using a Spatio-Temporal Encoding Technique Based on Frequency Division for Synthetic Transmit Aperture Ultrasound

Fredrik Gran and Jørgen Arendt Jensen, *Senior Member, IEEE*

***Abstract*—This paper investigates the possibility of flow estimation using spatio-temporal encoding of the transmissions in synthetic transmit aperture imaging (STA). The spatial encoding is based on a frequency division approach. In STA, a major disadvantage is that only a single transmitter (denoting single transducer element or a virtual source) is used in every transmission.**

The transmitted acoustic energy will be low compared to a conventional focused transmission in which a large part of the aperture is used. By using several transmitters simultaneously, the total transmitted energy can be increased. However, to focus the data properly, the signals originating from the different transmitters must be separated. To do so, the pass band of the transducer is divided into a number of subbands with disjoint spectral support. At every transmission, each transmitter is assigned one of the subbands. In receive, the signals are separated using a simple filtering operation. To attain high axial resolution, broadband spectra must be synthesized for each of the transmitters. By multiplexing the different waveforms on different transmitters over a number of transmissions, this can be accomplished. To further increase the transmitted energy, the waveforms are designed as linear frequency modulated signals. Therefore, the full excitation amplitude can be used during most of the transmission.

The method has been evaluated for blood velocity estimation for several different velocities and incident angles. The program Field II was used. A 128-element transducer with a center frequency of 7 MHz was simulated. The 64 transmitting elements were used as the transmitting aperture and 128 elements were used as the receiving aperture. Four virtual sources were created in every transmission. By beamforming lines in the flow direction, directional data were extracted and correlated. Hereby, the velocity of the blood was estimated. The pulse repetition frequency was 16 kHz. Three different setups were investigated with flow angles of 45, 60, and 75 degrees with respect to the acoustic axis. Four different velocities were simulated for each angle at 0.10, 0.25, 0.50, and 1.00 m/s. The mean relative bias with respect to the peak flow for the three angles was less than 2%, 2%, and 4%, respectively.

I. Introduction

Synthetic transmit aperture (STA) can be used for velocity estimation in ultrasound imaging [1]–[5]. The method is based on correlating data acquired with exactly the same emission sequence. To synthesize a large transmit aperture, several transmissions have to be carried out from different locations on the transmitting aperture. Beamforming the received signals from one transmission results in a low resolution image with poor resolution and contrast. The synthesis of a larger transmit aperture is achieved by summing data from different transmissions yielding a high-resolution image. This improves the resolution and contrast as well as the image quality.

If the object under investigation is moving very rapidly only a small number of transmissions is affordable. Having a large number of transmissions to generate a high resolution image would yield poor performance of the velocity estimator because the movement results in a smearing of the point spread function (PSF). When the number of transmissions per data set is small, the signal-to-noise-ratio (SNR), however, will drop. Virtual sources have been suggested to partly compensate for this [6]–[9]. Temporal encoding in the form of a linear frequency modulated signal also has been suggested to increase the SNR [10]–[17].

Spatial encoding has been suggested as a means of increasing SNR for STA when the number of transmissions per high-resolution image is low. Chiao *et al.* [18] suggested that a Hadamard space-time encoding scheme could be used to encode the transmitters[1]. The method relies on exciting the transmitters simultaneously with the same excitation waveforms. The encoding is based on premultiplying the waveform on each transmitter by a row (or column) of the Hadamard matrix of the same dimension as the number of transmitters (2^k). The next transmission is premultiplied by the next row, and this procedure is repeated until all rows have been covered. Under the assumption of static target geometry, the echoes originating from the different transmitters can be extracted by summing and subtracting the received signals from the different transmissions. The target geometry has to be static from transmission to transmission, for the decoding to work properly. In flow estimation the target is not static, and it has been argued that this would degrade the method, making it unsuitable for flow imaging.

Manuscript received June 17, 2005; accepted January 20, 2006. This work was supported by grant 9700883, 9700563 and 26-01-0178 from the Danish Science Foundation and by B-K Medical A/S, Denmark.

The authors are with the Center for Fast Ultrasound Imaging, Ørsted•DTU, Technical University of Denmark, 2800 Kgs. Lyngby, Denmark (e-mail: fg@oersted.dtu.dk).

[1]The general term transmitter will be used to represent a virtual source or a single transducer element. In [18] this was called phase center.

Chiao and Thomas suggested in [19] to use complementary codes (orthogonal Golay sequences) to encode the transmitters. Here the transmitters are assigned a specific binary code sequence for each transmitter, and correlation receivers are applied to separate the signals. From one transmission the intercode cross correlation is not zero, but by summing the result from different transmission using different code sequences, the inter-code, cross correlation can be made to vanish. Using the same procedure, perfect auto-correlation properties can be achieved for the combined auto-correlation functions. This approach also assumes static target geometry as data from different transmissions have to be combined.

In this paper a method for spatial encoding developed in [20]–[22] is evaluated for blood flow estimation as suggested in [23]. To focus the data properly, the information originating from the different transmitters must be separated. To do so, the pass band of the transducer is divided into a number of subbands with disjoint spectral support. At every transmission, each transmitter is assigned one of the subbands. In receive, the signals are separated using a simple filtering operation. The decoding can be performed instantaneously at the receiver, making the decoding process insensitive to motion. To attain high-axial resolution, broadband spectra must be synthesized for each of the transmitters. This can be accomplished by multiplexing the different waveforms on different transmitters over a number of transmissions. Although the decoding is insensitive to motion, the synthesis of the broadband spectra, however, may exhibit motion artifacts as further detailed in Section VI. To further increase the transmitted energy, the waveforms are designed as linear frequency modulated signals.

The paper is organized as follows. In Section II the spatial coding is described, in Section III the beamforming, which was applied to create directional flow data, is explained. In Section IV the estimation procedure for finding the velocity of the blood is given. The simulation setup is described in Section V, and in Section VI the effects of motion on the broadband synthesis is analyzed. In Section VII the simulation results are presented and discussed. Concluding remarks are given in Section VIII.

II. Spatial Encoding Using Frequency Division

Spatial encoding using frequency division has been shown to improve the SNR for stationary objects (tissue mimicking phantoms) [21], [22]. To separate the signals originating from the different transmitters, narrow-band signals with disjoint spectral support[2] are designed. To exploit the full excitation voltage of the system, the signals are designed as linear-frequency modulated signals:

$$s_i(t) = b(t)\sin\left(2\pi\left[\left(f_i - \frac{B}{2}\right)t + \frac{B}{2T}t^2\right]\right), \quad 0 \le t \le T, \tag{1}$$

where f_i is the center frequency of the i:th waveform, B is the bandwidth, T is the duration of the waveform, and $b(t)$ is a temporal weighting applied to the waveform. The compression and separation filters for each individual waveform are given by:

$$m_i(t) = s_i(-t) \star h_i(t), \tag{2}$$

where $\star$ denotes the convolution operator and $h_i(t)$ is an additional filter applied to shape the synthesized broadband spectrum. Consider the filtered i:th waveform:

$$r_i(t) = s_i(t) \star m_i(t) = s_i(t) \star s_i(-t) \star h_i(t), \tag{3}$$

with the Fourier transform

$$\mathcal{F}\{r_i(t)\} = |S_i(f)|^2 H_i(f), \tag{4}$$

where $S_i(f)$ is the Fourier transform of $s_i(t)$ and $H_i(f)$ is the Fourier transform of $h_i(t)$. The spectrum $H_i(f)$ is chosen such that the combined spectrum for the different signals produce a smooth broadband spectrum. In this paper, $H_i(f)$ was chosen to be:

$$H_i(f) = \begin{cases} \frac{1}{2}\left(1 + \cos\left(2\pi\dfrac{f - f_i}{B}\right)\right) & |f - f_i| \le \frac{B}{2} \\ 0 & \text{otherwise,} \end{cases} \tag{5}$$

as these spectra combined, $\sum_i H_i(f)$ give a broadband spectrum with a smooth passband. The filters $h_i(t)$ were designed as linear-phase finite impulse response (FIR) filters in which the filter coefficients were optimized using least-squares error minimization[3]. In this paper, eight waveforms were generated. The duration was 25 μs, the bandwidth was 2 MHz, and the function $b(t)$ was chosen to be a Tukey-window with 35% tapering. The Tukey window is defined as:

$$b(t) = \begin{cases} \frac{1}{2}\left(1 + \cos\left[2\pi\dfrac{t - \frac{\alpha}{2}T}{\alpha T}\right]\right) & 0 \le t \le \frac{\alpha T}{2} \\ 1 & \frac{\alpha T}{2} \le t \le \left(1 - \frac{\alpha}{2}\right)T, \\ \frac{1}{2}\left(1 + \cos\left[2\pi\dfrac{t - \left(1 - \frac{\alpha}{2}\right)T}{\alpha T}\right]\right) & \left(1 - \frac{\alpha}{2}\right)T \le t \le T \end{cases} \tag{6}$$

where T is the duration of the window and $\alpha = 0.35$ is the amount of tapering applied. The center frequencies can be seen in Table I. To reduce intersignal interference caused by overlapping frequencies, the waveforms were grouped in two sets. The first signal set consisted of the signals with odd index and the second set of the signals with even index. This makes it possible to encode four transmitters simultaneously, but it requires eight transmissions before a broadband spectrum can be synthesized for each transmitter. The two signal sets can be seen in Fig. 1. The filters $h_i(t)$ were specified to be FIR filters with a duration of 18.75 μs. The synthesized broadband time signal for one transmitter can be seen in Fig. 2. The majority of the

[2]This is only an approximation. The waveforms will not have disjoint spectral support in practice as this would require that infinite code sequences were used.

[3]Using the function `firls` in Matlab, ©1994–2005 by The MathWorks, Inc., Natick, MA 01760-1500.

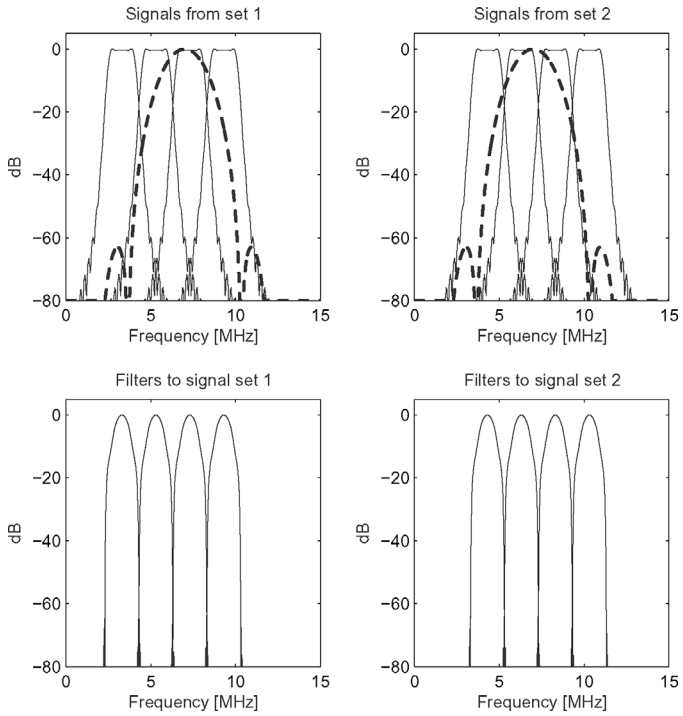

Fig. 1. The spectra for the two sets of excitation signals can be seen as the top figure. The corresponding separation filters are given as the two bottom figures. Note how the FIR filters $h_i(t)$ effect the frequency characteristic of the matched filters. The FIR filters reduce the inter-transmitter interference and shapes the filtered spectrum of each transmitter.

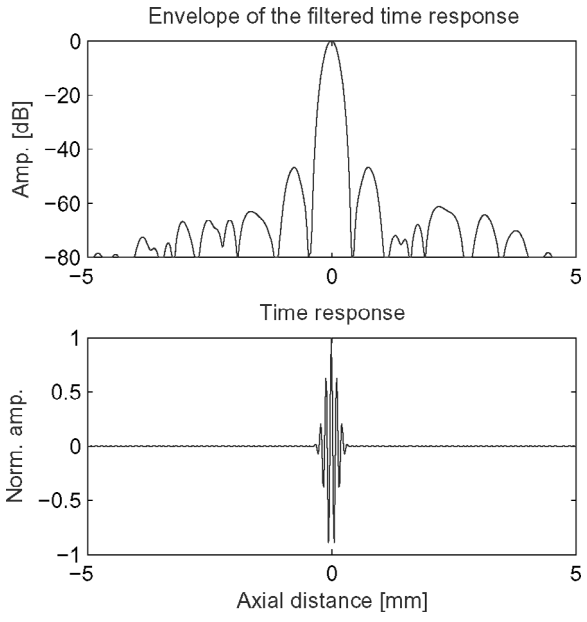

Fig. 2. The time response of a synthesized broadband pulse. After eight transmissions, broadband pulses can be synthesized for each transmitter. The axial sidelobe level is below −60 dB except for the near sidelobes which have a level of ∼ −50 dB. The top figure displays the log compressed envelope of the time signal. The bottom figure displays the actual time response on a linear scale.

TABLE I
THE CENTER FREQUENCIES OF THE DIFFERENT WAVEFORMS.

i	f_i [MHz]
1	3.3000
2	4.3512
3	5.4024
4	6.4536
5	7.5048
6	8.5560
7	9.6072
8	10.6584

axial sidelobes are below −60 dB, with exception for the near sidelobes that are at ∼ −50 dB. This is acceptable in a STA system used for flow estimation because the short transmission sequence used to synthesize the transmitting aperture will cause the lateral sidelobes to have a level of ∼ −40 dB.

III. BEAMFORMING

This section describes the beamforming that has been applied to properly focus the data. When a broadband excitation signal has been synthesized for every transmitter on the aperture, it is possible to beamform the synthesized broadband data as if only one transmitter was active in every transmission. This allows the synthetic aperture focusing technique described in [24] to be applied.

Because the system has access to defocused transmissions from all transmitters on the aperture, it is possible to focus the acoustic energy on any arbitrarily chosen point of interest. The amplitude in a point $\vec{r}_p$ in the image is given by:

$$\mathbf{H}\left(\vec{r}_p\right) = \sum_{k=1}^{K}\sum_{q=1}^{Q} a_q\left(t_{pkq}\right) r_{kq}\left(t_{pkq}\right), \tag{7}$$

where $a_q(t_{pkq})$ is a weighting function (apodization) over the receiving aperture, which ideally would be changing with spatial coordinates to keep a constant F-number. However, in this paper the apodization is constant over space and is chosen as a Hanning window over all 128 receiving elements. The time signal $r_{kq}(t)$ is the received synthesized broadband echo on the q:th receiver, originating from the k:th transmitter. Here t_{pkq} is the time corresponding to the geometrical travel distance from the k:th transmitter to the point $\vec{r}_p$ and back to the q:th receiver:

$$t_{pkq} = \frac{\left\|\vec{r}_p - \vec{r}_{\mathrm{xmt},k}\right\| + \left\|\vec{r}_{\mathrm{rcv},q} - \vec{r}_p\right\|}{c}, \tag{8}$$

where c is the speed of sound, and $\vec{r}_p - \vec{r}_{\mathrm{xmt},k}$ is the vector from the transmitter to the point $\vec{r}_p$, and $\vec{r}_{\mathrm{rcv},q} - \vec{r}_p$ is the vector from the point $\vec{r}_p$ to the receiver as indicated in Fig. 3. The beamformed data resulting from one transmission is denoted low-resolution image, and the result of

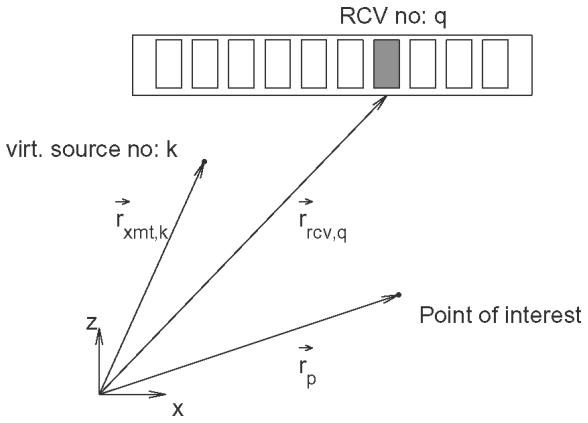

Fig. 3. Principles of synthetic aperture focusing for a point $\vec{r}_p$ for the k:th transmitter and the q:th receiver.

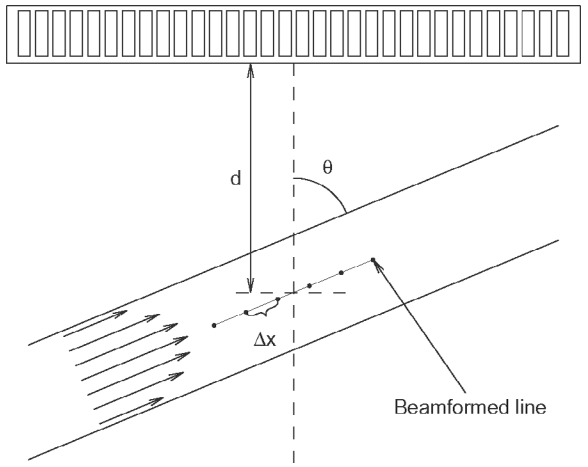

Fig. 4. The vessel is positioned at a depth $d = 30$ mm below the transducer. The angle of the flow with respect to the central axis of the transducer is indicated by θ. The radius of the vessel was 5 mm. To acquire directional data, points along the direction of the flow were beamformed. The direction of the flow was assumed to be known.

summing a number of low-resolution images to synthesize a larger aperture results in a high-resolution image. Summing contributions from all transmissions for all receiving elements gives both dynamic transmit and receive focusing.

To obtain directional data suitable for finding the velocity of the moving particles, lines were beamformed in the direction of the flow [25], [26]. The principle can be seen in Fig. 4. Correlating successive lines, the spatial shift between the data can be found and, thus, the velocity. The spatial distance between data points in the directional data was chosen to be $\Delta x = \lambda/10$. Moreover, it previously was shown that automatic detection of the flow angle is possible [5], [27]. Therefore, the angle of the flow was assumed to be known.

IV. Velocity Estimator

The velocity of the moving blood scatterers was found using a cross-correlation velocity estimator [28], [29]. No stationary signal was present; therefore, stationary echo canceling was ignored. However, it should be noted that, if a stationary echo-canceling filter would be applied, the results may degrade. This is going to be a subject for further investigation.

Because four transmitters were used, eight transmissions had to be carried out before broad-band spectra could be synthesized for each transmitter. The velocity was found by correlating lines that had been beamformed in the direction of the flow. To find the velocity, lines obtained using the same transmission were correlated. A line in the l:th high-resolution image is denoted $h_l(n)$, and the corresponding line in the next high-resolution image obtained with the same transmission sequence is denoted $h_{l+1}(n)$. The cross correlation between the lines is:

$$R(m) = \frac{1}{N}\sum_{n=0}^{N-1} h_l(n)h_{l+1}(n+m), \tag{9}$$

where N is the length of the lines in samples. The spatial shift between two high-resolution lines was found by finding the peak in the cross-correlation function:

$$m_{\max} = \arg\max_m R(m). \tag{10}$$

To get a more precise result, quadratic interpolation was performed using the samples $(m_{\max} - 1,\ m_{\max},\ m_{\max} + 1)$. The maximum lag[4] resulting from the interpolation is given by [29], [30]:

$$m_v = m_{\max} - \frac{R(m_{\max}+1) - R(m_{\max}-1)}{2\left(R(m_{\max}+1) - 2R(m_{\max}) + R(m_{\max}-1)\right)}. \tag{11}$$

The velocity was found:

$$v_{\max} = \frac{m_v \Delta x}{T_h}, \tag{12}$$

where Δx is the spatial distance between samples in the high-resolution lines, and T_h is the time period between two successive, high-resolution images obtained with the same transmission sequence[5].

V. Simulation Setup

The method has been evaluated using the simulation tool Field II [31], [32]. A 128-element, linear-array transducer was used with the parameters shown in Table II. The central 64 transducer elements were used as the transmitting aperture, and 128 elements were active as the receiving aperture. Four virtual sources were created [6]–[9], [33]. A virtual source was created by focusing 16 transducer elements 5 mm behind the face of the transducer. The purpose was to emulate a high-energy virtual spherical source. The basic principle can be seen in Fig. 5. The different

[4]May be fractional.

[5]In this paper $T_h = 8/f_{pr}$ because eight emissions were used to create a high-resolution image.

TABLE II
DIFFERENT PARAMETERS USED IN THE SIMULATION.

Variable	Parameter	Unit
f_{pr}	16	kHz
f_0	7	MHz
λ	0.2200	mm
pitch	0.2080	mm
height	4.5	mm
No xmt elem.	64	
No rcv elem.	128	
No virt. sources	4	
Focal depth	-5	mm
Δx	1/10	λ
Line length	20	λ
Vessel radius	5	mm
Depth of vessel	30	mm

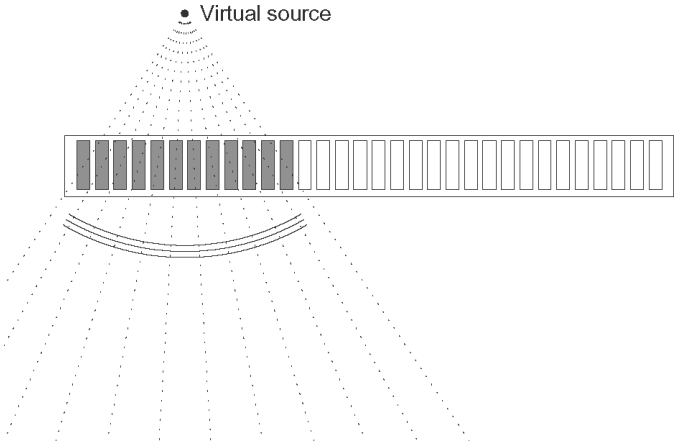

Fig. 5. The virtual source is created using 16 adjacent transducer elements. The focal point was chosen to 5 mm behind the face of the transducer (F-number 1.5). Hereby, a high-energy, virtual-spherical wave was created.

waveforms were multiplexed for the different transmitters over eight transmissions. The transmission sequence used for the velocity estimation can be seen in Table III.

The pulse repetition frequency was 16 kHz; therefore, 2000 high-resolution images suitable for velocity estimation were created every second. The vessel was created as a cylinder with a radius of 5 mm, at a depth of 30 mm to the center of the vessel relative to the transducer. The length of the vessel was 20 mm, and enough point scatterers were positioned inside the vessel to ensure that 10 scatterers occupied a resolution cell[6]. The flow was laminar with a parabolic flow profile:

$$v(r) = v_{\max}\left(1 - \left(\frac{r}{R}\right)^2\right), \tag{13}$$

where $v_{\max}$ is the peak velocity, R is the radius of the vessel, and r is the location in the vessel where the velocity should be evaluated. The parameters for the simulation can be seen in Table II.

[6]A resolution cell was assumed to be $\lambda \times \lambda \times \lambda$.

TABLE III
THE TRANSMISSION SEQUENCE USED FOR THE FLOW ESTIMATION, XMT NO. DENOTES THE TRANSMITTER OF INTEREST AND EM. NO. IS THE EMISSION NUMBER.

XMT No. / Em. No.	1	2	3	4
1	1	3	5	7
2	2	4	6	8
3	7	1	3	5
4	8	2	4	6
5	5	7	1	3
6	6	8	2	4
7	3	5	7	1
8	4	6	8	2

VI. MOTION EFFECTS BROADBAND SYNTHESIS

To evaluate the SNR, consider the following very simple model of the received signal:

$$r(t) = p(t) \star h(t) + v(t), \tag{14}$$

where $p(t)$ is the combined filtered waveforms influenced by motion as depicted in Fig. 6, and $h(t)$ is a function representing the interaction between the wave and the interrogated tissue[7]. The function $h(t)$ is modeled as a Gaussian distributed, white process with zero mean. The variable $v(t)$ is the filtered measurement noise and is assumed to be independent of the signal. The SNR then is given as:

$$\mathrm{SNR} = \frac{E\left[|p(t) \star h(t)|^2\right]}{E\left[|v(t)|^2\right]}, \tag{15}$$

where $E[(\cdot)]$ is the expectancy value of $(\cdot)$. Now, consider the autocorrelation of $p(t) \star h(t)$:

$$R_{ph}(\tau) = R_p(\tau) \star R_h(\tau), \tag{16}$$

where $R_p(\tau)$ and $R_h(\tau)$ are the autocorrelation functions of $p(t)$ and $h(t)$, respectively. By using the fact that $h(t)$ is modeled as a white Gaussian distributed process with zero mean, the autocorrelation function of $h(t)$ can be written:

$$R_h(\tau) = S_h\delta(\tau), \tag{17}$$

where S_h is the power spectral density of $h(t)$. Combining (16) and (17) gives:

$$R_{ph}(\tau) = S_h R_p(\tau). \tag{18}$$

The numerator in (15) is (18) evaluated at $\tau = 0$; (18) evaluated at $\tau = 0$ gives:

$$R_{ph}(0) = S_h R_p(0) = S_h \cdot E_p, \tag{19}$$

[7]This assumes that the movement is uniform over the target function and purely axial to the transmitter and the receiver of interest.

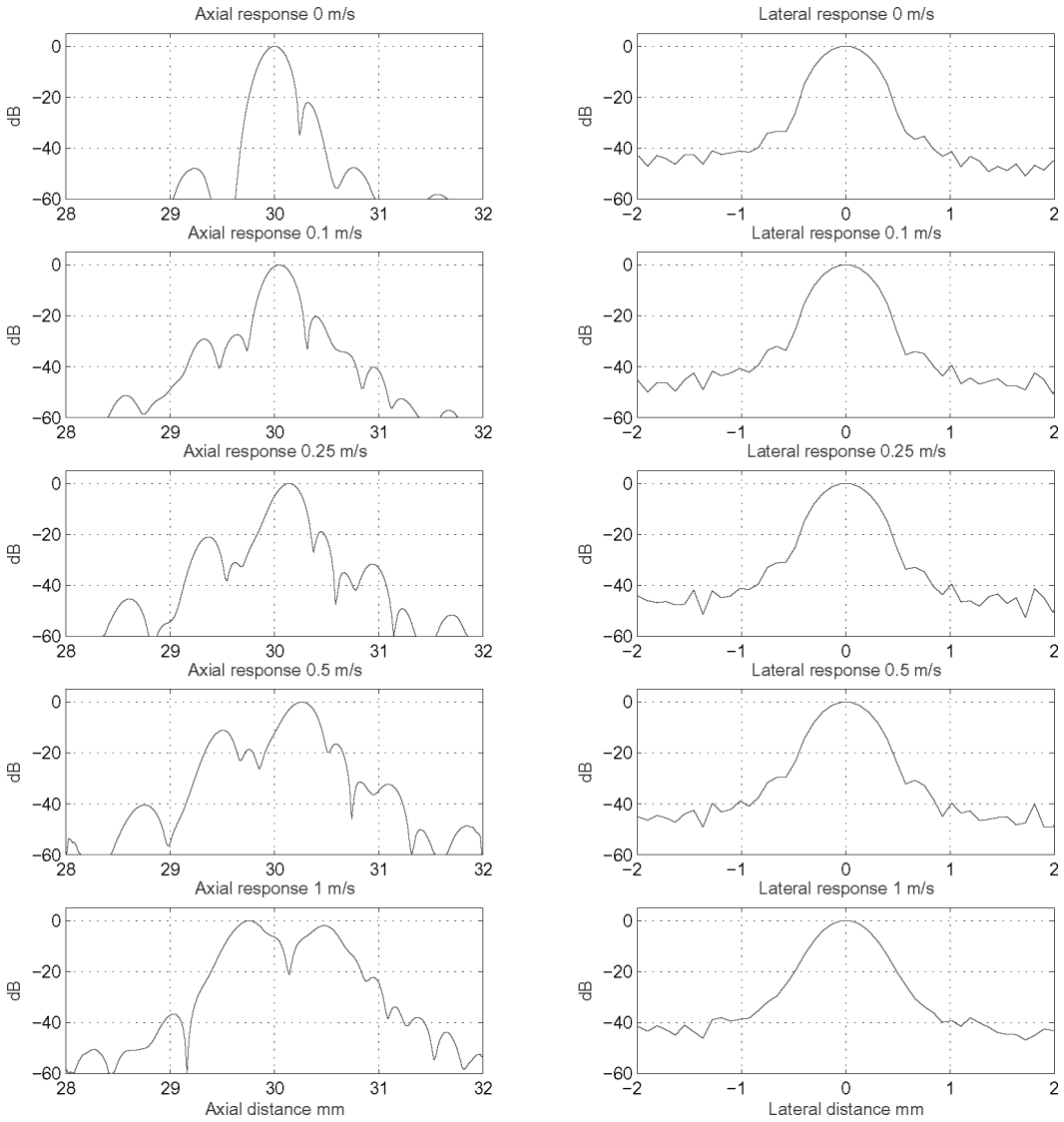

Fig. 6. The synthesized broadband beamformed response as a function of velocity. The target is a single point scatterer located at a depth of 30 mm on the central axis of the transducer. The synthesized pulse is valid for the second virtual source. The graphs to the left represent the axial response, and the graphs to the right represent the lateral response.

where E_p is the energy of $p(t)$. The decrease in SNR for a moving target with the synthesized broadband pulse having energy E_{mov}, compared to a stationary target with a synthesized broadband pulse with energy E_{stat} is (in logarithmic scale):

$$10 \log_{10} \left(\frac{E_{\text{mov}}}{E_{\text{stat}}} \right), \tag{20}$$

because the variance of the filtered noise is assumed to be the same for the two situations as well as the power spectral density of $h(t)$. Eq. (20) is evaluated as a function of velocity for the synthesized broadband pulses in Fig. 7.

VII. Simulation Results

The directional lines were beamformed and extracted. Succeeding high-resolution lines acquired using the same transmission sequence were correlated. To improve the estimates, 10 successive estimates for the cross-correlation function were averaged, so that 80 transmissions were used to generate one velocity estimate. The peak of the averaged cross-correlation function was found, and thereby the velocity was estimated. Table IV shows the angles and velocities that were investigated. To evaluate performance, bias and standard deviation were calculated for the estimates of the velocity for the different simulation setups.

TABLE IV
The Flow Angles and Velocities Included in the Study.

Angle	Velocities	Unit
45°	0.10, 0.25, 0.50, 1.00	m/s
60°	0.10, 0.25, 0.50, 1.00	m/s
75°	0.10, 0.25, 0.50, 1.00	m/s

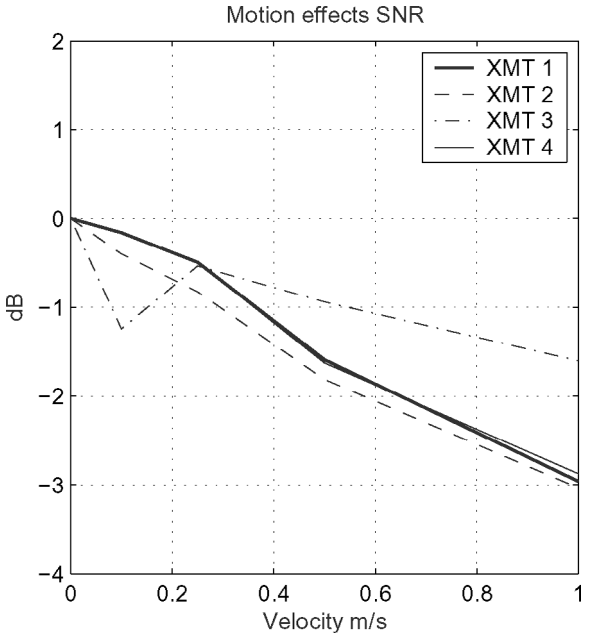

Fig. 7. The SNR as a function of velocity for the four different virtual sources. The SNR is decreased by 3 dB when the target is moving with a velocity of 1 m/s.

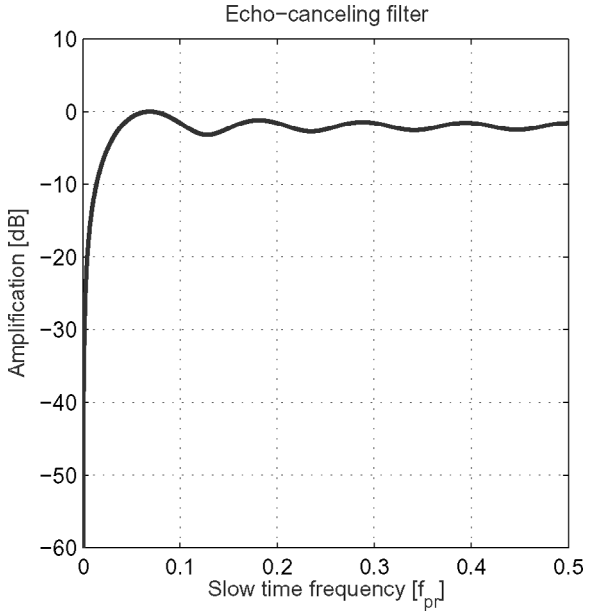

Fig. 8. The amplitude spectrum of the echo-canceling filter applied to the slow-time data.

For each setup, 22 full velocity[8] estimates were used to calculate the bias and standard deviation. The mean of the velocity estimates is given by:

$$\overline{v}(z) = \frac{1}{M}\sum_{m=0}^{M-1}\hat{v}_m(z), \tag{21}$$

where $\hat{v}_m(z)$ is the m:th estimate for the velocity. The total number of estimates is given by M. The bias for the estimates is given by (as a function of depth):

$$b(z) = \overline{v}(z) - v(z), \tag{22}$$

where $\hat{v}(z)$ is the estimate for the velocity at the depth z and $v(z)$ is the true velocity for this depth. The standard deviation for the estimates is given by:

$$\sigma(z) = \sqrt{\frac{1}{M}\sum_{m=0}^{M-1}[\hat{v}_m(z) - \overline{v}(z)]^2}. \tag{23}$$

The mean relative bias and the mean relative standard deviation are given by the mean bias and standard deviation relative to the peak velocity in the vessel. Mean relative bias (in percent):

$$\overline{b}_{\text{rel}} = \frac{1}{v_{\max}}\left(\frac{1}{Z}\sum_{z=0}^{Z-1} b(z)\right)\cdot 100\%, \tag{24}$$

where the samples $z = 0, \ldots, Z-1$ are the samples within the vessel. Mean relative standard deviation (in percent):

$$\overline{\sigma}_{\text{rel}} = \frac{1}{v_{\max}}\sqrt{\left(\frac{1}{Z}\sum_{z=0}^{Z-1}\sigma^2(z)\right)}\cdot 100\%, \tag{25}$$

where z is the sample index indicating where in the vessel the standard deviation is evaluated, and $z = 0, \ldots, Z-1$ are the samples within the vessel. The results for the velocity estimation for 45° for the four different velocities can be seen in Figs. 9–12.

The corresponding mean relative bias for the different velocities is depicted in Fig. 16 as the solid line. The bias is below 2% in all four simulations. The standard deviation depicted in Fig. 17 as the solid line is significantly higher for the simulation with a peak velocity of 1 m/s. This can be explained by examining Fig. 12, which displays several false peaks in the velocity estimation. The result for the velocity estimation for 60° for the simulation with a peak velocity of 1 m/s can be seen in Fig. 13.

The mean relative bias for the four different velocities at 60° is shown in Fig. 16 as the dashed line. The bias is below 2% in all four simulations. The mean relative standard deviation given in Fig. 17 tends to drop for higher velocities. It should, however, be noted that the absolute standard deviation is higher for the higher velocities. The result for the velocity estimation for 75° for the simulation with peak velocity of 1 m/s can be seen in Fig. 15. The mean relative bias for the different velocities is given in Fig. 16 as the dotted line. The bias is below 4% in all four simulations. The mean relative standard deviation given in Fig. 17 tends again to drop for higher velocities. However, once again the absolute standard deviation is higher for the higher velocities.

The influence of applying a stationary echo canceling filter was investigated for the setup with 60° flow angle

[8]Each velocity estimate was based on 10 successive, high-resolution images.

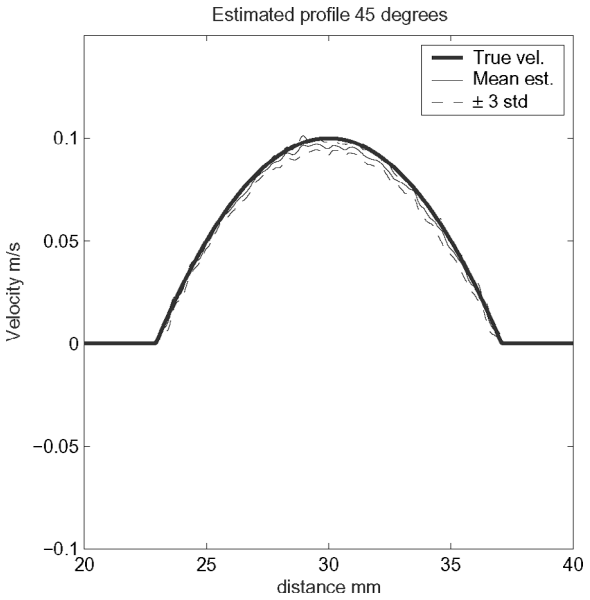

Fig. 9. The estimated velocity as a function of depth. The angle of the flow relative to the central axis of the transducer was 45°. The flow had a parabolic velocity distribution over the vessel with peak velocity 0.1 m/s.

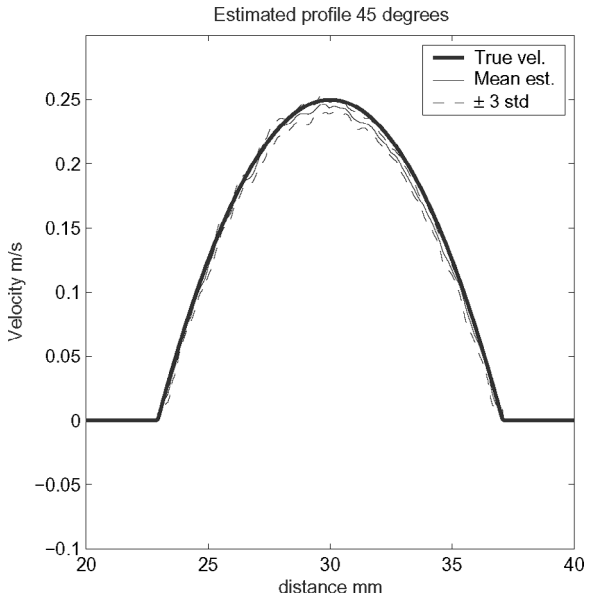

Fig. 10. The estimated velocity as a function of depth. The angle of the flow relative to the central axis of the transducer was 45°. The flow had a parabolic velocity distribution over the vessel with peak velocity 0.25 m/s.

TABLE V
THE MEAN RELATIVE BIAS AND STANDARD DEVIATION IN PERCENT BEFORE (LEFT COLUMN) AND AFTER (RIGHT COLUMN) THE ECHO-CANCELING FILTER WAS APPLIED.

	Without echo-canc.	With echo-canc.
Rel. bias	1.32%	1.26%
Rel. std.	0.407%	0.399%

and peak velocity 1 m/s. The echo-canceling filter was a running mean subtraction filter:

$$h_l^{ec}(n) = h_l(n) - \frac{1}{K}\sum_{k=0}^{K-1} h_{l-k}(n), \tag{26}$$

where K is the duration of the filter in slow time and $h_l^{ec}(n)$ is the l:th echo-canceled, high-resolution line. The amplitude spectrum of this filter can be seen in Fig. 8. In this investigation $K = 10$. The velocity estimation was repeated, and the result from this simulation can be seen in Fig. 14. It can be seen that the estimated profile does not change drastically. When comparing the mean relative bias and standard deviation, it was found that both were actually improved after echo-canceling, as can be seen in Table V.

VIII. CONCLUSIONS

This paper has investigated the feasibility to use spatial encoding of the transmits by means of frequency division for velocity estimation. A simulation study was carried out where a vessel with a radius of 5 mm was scanned at a depth of 30 mm. Several different velocities were tested, 0.1, 0.25, 0.50, and 1.00 m/s. Three angles were scanned per velocity 45°, 60°, and 75°. The mean bias relative to the peak velocity was for 45° less than 2%, for 60° less than 2% and for 75° less than 4%. Therefore, it is concluded that it is possible to estimate blood velocities using spatial encoding of the transmitters based on frequency division. This makes it possible to exploit the benefits of using spatial encoding in blood flow estimation, which would not be possible with, e.g., Hadamard encoding.

REFERENCES

[1] S. I. Nikolov and J. A. Jensen, "Velocity estimation using synthetic aperture imaging," in *Proc. IEEE Ultrason. Symp.*, 2001, pp. 1409–1412.

[2] J. A. Jensen and S. I. Nikolov, "Transverse flow imaging using synthetic aperture directional beamforming," in *Proc. IEEE Ultrason. Symp.*, 2002, pp. 1488–1492.

[3] S. I. Nikolov and J. A. Jensen, "In-vivo synthetic aperture flow imaging in medical ultrasound," *IEEE Trans. Ultrason., Ferroelect., Freq. Contr.*, vol. 50, no. 7, pp. 848–856, 2003.

[4] J. A. Jensen and S. I. Nikolov, "A method for real-time three-dimensional vector velocity imaging," in *Proc. IEEE Ultrason. Symp.*, 2003, pp. 1582–1585.

[5] J. A. Jensen, "Velocity vector estimation in synthetic aperture flow and B-mode imaging," in *IEEE Int. Symp. Biomed. Imaging from Nano to Macro*, 2004, pp. 32–35.

[6] M. O'Donnell and L. J. Thomas, "Efficient synthetic aperture imaging from a circular aperture with possible application to catheter-based imaging," *IEEE Trans. Ultrason., Ferroelect., Freq. Contr.*, vol. 39, pp. 366–380, 1992.

[7] M. Karaman, P. C. Li, and M. O'Donnell, "Synthetic aperture imaging for small scale systems," *IEEE Trans. Ultrason., Ferroelect., Freq. Contr.*, vol. 42, pp. 429–442, 1995.

[8] C. H. Frazier and W. D. O'Brien, "Synthetic aperture techniques with a virtual source element," *IEEE Trans. Ultrason., Ferroelect., Freq. Contr.*, vol. 45, pp. 196–207, 1998.

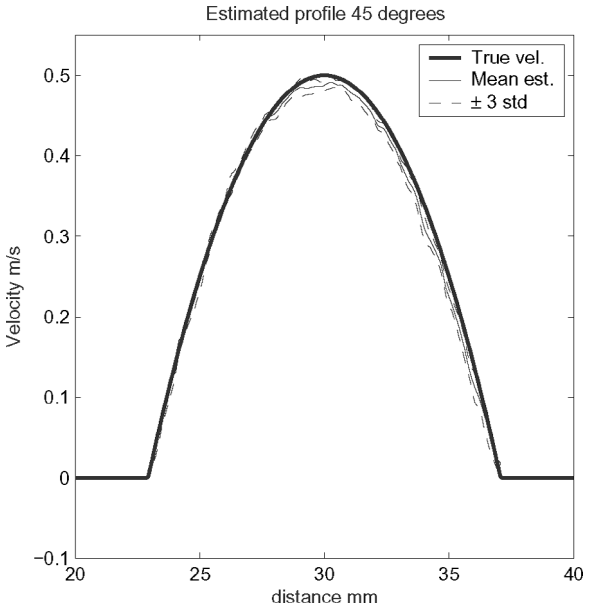

Fig. 11. The estimated velocity as a function of depth. The angle of the flow relative to the central axis of the transducer was 45°. The flow had a parabolic velocity distribution over the vessel with peak velocity 0.50 m/s.

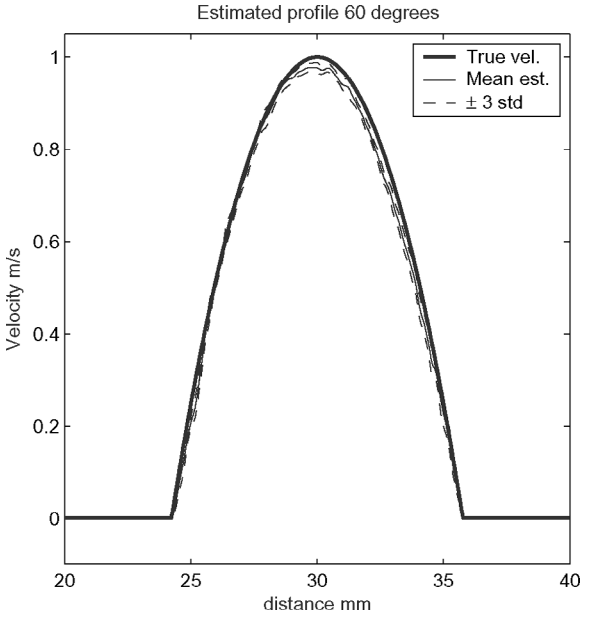

Fig. 13. The estimated velocity as a function of depth. The angle of the flow relative to the central axis of the transducer was 60°. The flow had a parabolic velocity distribution over the vessel with peak velocity to 1.00 m/s.

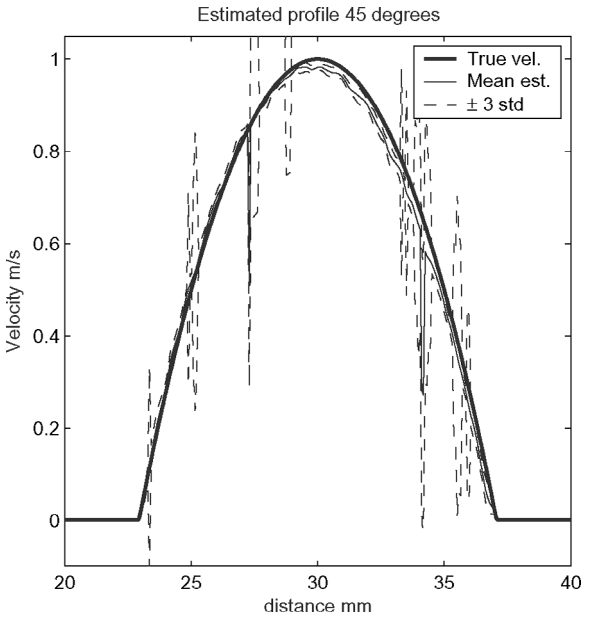

Fig. 12. The estimated velocity as a function of depth. The angle of the flow relative to the central axis of the transducer was 45°. The flow had a parabolic velocity distribution over the vessel with peak velocity to 1.00 m/s.

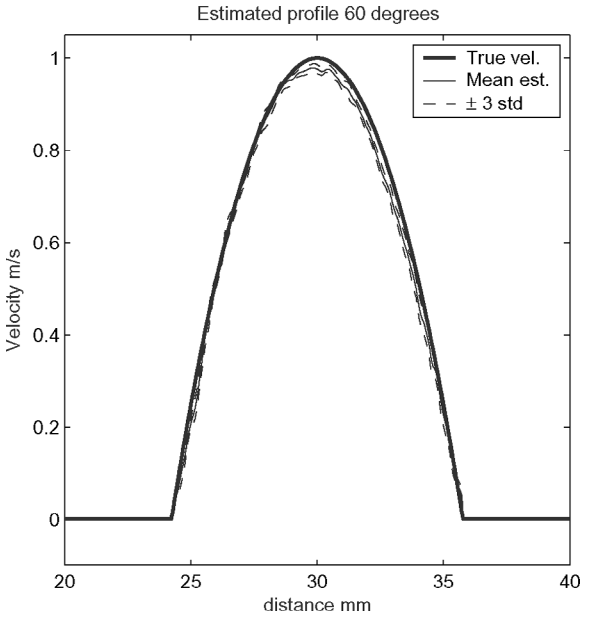

Fig. 14. The estimated velocity as a function of depth for the echo-cancelled data. The angle of the flow relative to the central axis of the transducer was 60°. The flow had a parabolic velocity distribution over the vessel with peak velocity 1.00 m/s.

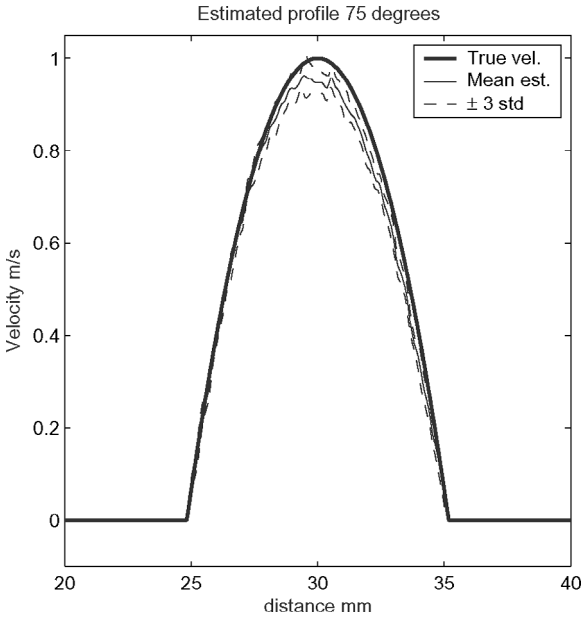

Fig. 15. The estimated velocity as a function of depth. The angle of the flow relative to the central axis of the transducer was 75°. The flow had a parabolic velocity distribution over the vessel with peak velocity 1.00 m/s.

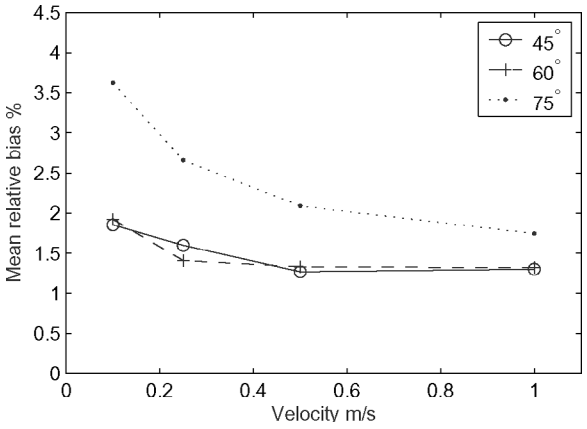

Fig. 16. The mean relative bias as a function of velocity. The solid line represents the results for 45°, the dashed line 60°, and the dotted line 75°.

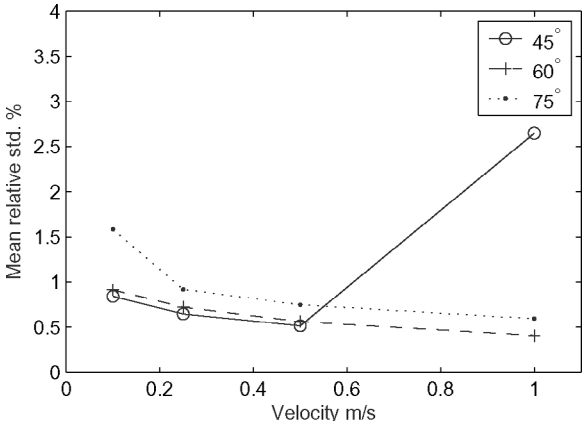

Fig. 17. The mean relative standard deviation as a function of velocity. The solid line represents the results for 45°, the dashed line 60°, and the dotted line 75°.

[9] M. H. Bae and M. K. Jeong, "A study of synthetic-aperture imaging with virtual source elements in B-mode ultrasound imaging systems," *IEEE Trans. Ultrason., Ferroelect., Freq. Contr.*, vol. 47, pp. 1510–1519, 2000.

[10] M. I. Skolnik, *Introduction to Radar Systems*. New York: McGraw-Hill, 1980.

[11] M. I. Skolnik, *Radar Handbook*. 2nd ed. New York: McGraw-Hill, 1990.

[12] M. O'Donnell, "Coded excitation system for improving the penetration of real-time phased-array imaging systems," *IEEE Trans. Ultrason., Ferroelect., Freq. Contr.*, vol. 39, pp. 341–351, 1992.

[13] T. X. Misaridis and J. A. Jensen, "An effective coded excitation scheme based on a predistorted FM signal and an optimized digital filter," in *Proc. IEEE Ultrason. Symp.*, 1999, pp. 1589–1593.

[14] T. Misaridis and J. A. Jensen, "Use of modulated excitation signals in ultrasound. Part I: Basic concepts and expected benefits," *IEEE Trans. Ultrason., Ferroelect., Freq. Contr.*, vol. 52, no. 2, pp. 192–207, 2005.

[15] T. Misaridis and J. A. Jensen, "Use of modulated excitation signals in ultrasound. Part II: Design and performance for medical imaging applications," *IEEE Trans. Ultrason., Ferroelect., Freq. Contr.*, vol. 52, no. 2, pp. 208–219, 2005.

[16] T. Misaridis and J. A. Jensen, "Use of modulated excitation signals in ultrasound. Part III: High frame rate imaging," *IEEE Trans. Ultrason., Ferroelect., Freq. Contr.*, vol. 52, no. 2, pp. 220–230, 2005.

[17] R. Y. Chiao and X. Hao, "Coded excitation for diagnostic ultrasound: A system developer's perspective," *IEEE Trans. Ultrason., Ferroelect., Freq. Contr.*, vol. 52, pp. 160–170, 2005.

[18] R. Y. Chiao, L. J. Thomas, and S. D. Silverstein, "Sparse array imaging with spatially encoded transmits," in *Proc. IEEE Ultrason. Symp.*, 1997, pp. 1679–1682.

[19] R. Y. Chiao and L. J. Thomas, "Synthetic transmit aperture using orthogonal golay coded excitation," in *Proc. IEEE Ultrason. Symp.*, 2000, pp. 1469–1472.

[20] F. Gran and J. A. Jensen, "Multi element synthetic aperture transmission using a frequency division approach," in *Proc. IEEE Ultrason. Symp.*, 2003, pp. 1942–1946.

[21] F. Gran and J. A. Jensen, "Frequency division transmission and synthetic aperture reconstruction," *IEEE Trans. Ultrason., Ferroelect., Freq. Contr.*, vol. 53, no. 5, pp. 900–911, 2006.

[22] F. Gran and J. A. Jensen, "Spatio-temporal encoding using narrow-band linearly frequency modulated signals in synthetic aperture ultrasound imaging," in *Proc. SPIE—Progress in Biomed. Opt. Imaging*, vol. 5750, pp. 405–416, 2005.

[23] J. A. Jensen, "Simulation of advanced ultrasound systems using field II," in *IEEE Int. Symp. Biomed. Imaging Nano to Macro*, 2004, pp. 636–639.

[24] S. I. Nikolov, "Synthetic aperture tissue and flow ultrasound imaging," Ph.D. dissertation, Ørsted•DTU, Technical Univ. Denmark, 2800, Lyngby, Denmark, 2001.

[25] J. A. Jensen, "Directional velocity estimation using focusing along the flow direction: I: Theory and simulation," *IEEE Trans. Ultrason., Ferroelect., Freq. Contr.*, vol. 50, no. 7, pp. 857–872, July 2003.

[26] J. A. Jensen and R. Bjerngaard, "Directional velocity estimation using focusing along the flow direction: II: Experimental investigation," *IEEE Trans. Ultrason., Ferroelect., Freq. Contr.*, vol. 50, no. 7, pp. 873–880, July 2003.

[27] N. Oddershede and J. A. Jensen, "Experimental investigation of synthetic aperture flow angle estimation," in *Proc. SPIE Medical Imaging meeting, Ultrasonic Imaging and Signal Processing*, vol. 5750, pp. 417–426, 2005.

[28] O. Bonnefous, "Statistical analysis and time processes applied to velocity measurement," in *Proc. IEEE Ultrason. Symp.*, 1989, pp. 887–892.

[29] J. A. Jensen, *Estimation of Blood Velocities Using Ultrasound: A Signal Processing Approach*. New York: Cambridge Univ. Press, 1996.

[30] S. G. Foster, "A pulsed ultrasonic flowmeter employing time domain methods," Ph.D. dissertation, Department of Electrical Engineering, University of Illinois, Urbana, IL, 1985.

[31] J. A. Jensen and N. B. Svendsen, "Calculation of pressure fields from arbitrarily shaped, apodized, and excited ultrasound trans-

ducers," *IEEE Trans. Ultrason., Ferroelect., Freq. Contr.*, vol. 39, pp. 262–267, 1992.
[32] J. A. Jensen, "Field: A program for simulating ultrasound systems," in *Med. Biol. Eng. Comp., 10th Nordic-Baltic Conf. Biomed. Imaging*, Suppl. 1, pt. 1, 1996, pp. 351–353.
[33] S. I. Nikolov and J. A. Jensen, "Virtual ultrasound sources in high-resolution ultrasound imaging," *Proc. SPIE—Progress in Biomed. Opt. Imaging*, vol. 3, pp. 395–405, 2002.
[34] K. L. Gammelmark and J. A. Jensen, "Duplex synthetic aperture imaging with tissue motion compensation," in *Proc. IEEE Ultrason. Symp.*, 2003, pp. 1569–1573.

Fredrik Gran earned his M.Sc. degree in engineering physics from Lund University, Sweden, in 2002 and the Ph.D. degree in electrical engineering from the Technical University of Denmark, Denmark, in 2005. He is currently a postdoctoral researcher at the Center for Fast Ultrasound Imaging at the Technical University of Denmark.

His research interests include spatial and temporal encoding in medical ultrasound and signal processing.

Jørgen Arendt Jensen (M'93–SM'02) earned his Master of Science in electrical engineering in 1985 and the Ph.D. degree in 1989, both from the Technical University of Denmark. He received the Dr.Techn. degree from the university in 1996. He has published a number of papers on signal processing and medical ultrasound and the book *Estimation of Blood Velocities Using Ultrasound*, Cambridge University Press, in 1996.

He is also developer of the Field II simulation program. He has been a visiting scientist at Duke University, Stanford University, and the University of Illinois at Urbana-Champaign. He is currently full professor of Biomedical Signal Processing at the Technical University of Denmark at Ørsted•DTU and head of Center for Fast Ultrasound Imaging. He has given courses on blood velocity estimation at both Duke University and University of Illinois and teaches biomedical signal processing and medical imaging at the Technical University of Denmark. He has given several short courses on simulation, synthetic aperture imaging, and flow estimation at international scientific conferences. He is also the co-organizer of a new biomedical engineering education program offered by the Technical University of Denmark and the University of Copenhagen. His research is centered around simulation of ultrasound imaging, synthetic aperture imaging and blood flow estimation, and constructing systems for such imaging.